A COMPUTATIONAL STUDY OF THERMAL CONDUCTIVITY OF FREE-STANDING H-BN STRUCTURES

A Thesis

by

MINGXIN DONG

Submitted to the Office of Graduate and Professional Studies of
Texas A&M University
in partial fulfillment of the requirements for the degree of

MASTER OF SCIENCE

Chair of Committee:	Tahir Cagin
Committee Members:	Xiaofeng Qian
	Sreeram Vaddiraju
Department Head:	Ibrahim Karaman

May 2020

Major Subject: Materials Science & Engineering

Copyright 2020 Mingxin Dong

ABSTRACT

The fact that hexagonal boron nitride (h-BN) has remarkable thermal transport property, mechanical property and chemical stability provides endless possibilities in nanoscale thermal device designing. In this study, we investigated the thermal conductivity of different h-BN structures. We first gave a brief literature review of former experimental and simulation results, the development of MD simulations, and thermal transport theory based on Fourier's law and Green-Kubo formalism. We then applied equilibrium molecular dynamic (EMD) approach. Tersoff potential and LJ potential are applied as the in-plane/interlayer force field, respectively. Results showed that the in-plane thermal conductivity of bulk h-BN is around 170W/mK, while the interlayer thermal conductivity is reduced to 5W/mK due to interlayer phonon scattering. Thermal conductivity of pristine monolayer is around 300W/mK on average. Different phonon vibration modes could be speculated from the heat flux auto-correlation function (HCACF). We also applied non-equilibrium molecular dynamics (NEMD) methods and compared the result with the result given by Green-Kubo formalism. Both methods could give reasonable values of thermal conductivity, yet for NEMD methods the local stability should be taken into consideration.

ACKNOWLEDGEMENTS

First, I would like to thank my advisor, Dr. Cagin, who has been a constant supporter, and wise guide through my graduate experience. He has inspired the core of this work and shown me the real meaning of thinking outside the box. Moreover, I would like to thank all my fellow graduate students in Dr. Cagin's group who have supported me throughout my graduate study at Texas A&M University, especially Lan Huang for introducing me to the world of materials simulation.

I would also like to thank my committee members, Dr. Qian, Dr. Vaddiraju, for their guidance and support throughout the course of this research. Thanks also go to my friends and colleagues and the department faculty and staff for making my time at Texas A&M University a great experience.

CONTRIBUTORS AND FUNDING SOURCES

Contributors

This work was supported by a thesis (or) dissertation committee consisting of Professor Tahir Cagin and Professor Xiaofeng Qian of the Department of Materials Science and Engineering and Professor Sreeram Vaddiraju of the Department of Chemical Engineering.

All work conducted for the thesis was completed by the student independently.

Funding Sources

There are no outside funding contributions to acknowledge related to the research and compilation of this document.

TABLE OF CONTENTS

Page

LIST OF FIGURES

LIST OF TABLES

1. INTRODUCTION

1.1. Motivation

Low-dimensional carbon-based honeycomb nanostructures, including carbon nanotubes and graphene nanoribbons are known for fascinating physical properties, making them promising in future applications, and have also triggered broad interest in exploring the properties of their isomorphic materials such as hexagonal boron nitride (h-BN) structures. The fact that h-BN has remarkable thermal transport property, mechanical property and chemical stability provides endless possibilities in nanoscale thermal device designing. Despite the fact that a number of studies have been conducted, the thermal transport mechanism in h-BN is still not clear. The calculation results of h-BN thermal conductivity also have some inconsistencies.

It is known that the interactions between particles is determinant to material properties. Therefore, studies on atomic level are essential to better analyze and design nano-scale thermal transport devices. To serve this purpose, molecular dynamics (MD) approaches have been developed and applied to simulate the properties of materials. Since MD simulations could directly reflect the evolution of micro-structures and record information of each particle, they are meant to shed light on understanding experimental results as well as validating theoretical models.

In this research, theoretical models based on Fourier's law and Green-Kubo formalism are investigated to calculate the thermal conductivity of various h-BN systems, including multi-layer h-BN, pristine h-BN monolayer, h-BN monolayer with point defects and grain boundaries. The size effect on thermal conductivity is also considered. We also discussed the influence of different simulation methods.

1.2. Research Background

1.2.1 Experimental results

In order to fully understand the mechanism of thermal transport, numerous experiments and theoretical analysis of h-BN thermal transport properties have been conducted. L. Duclaux et al [1] prepared AA-stacked pyrolytic h-BN samples with size of approximately $25 \times 10 \times 1mm^3$ by chemical vapor deposition (CVD) method. The measured in-plane thermal conductivity ranges from 150 to 220 W/mK at room temperature. Jo et al [2] measured the thermal conductivity of suspended few-layer h-BN. These samples are exfoliated from PMMA substrates. It turned out that thermal conductivity of 11-layer h-BN could reach 360 W/mK, comparable to the bulk value. They also concluded that the thermal conductivity of suspended h-BN can approach to that of bulk h-BN crystals at room temperature when the thickness is larger than 10 atomic layers. According to Sichel et al [3], the thermal conductivity of bulk pyrolytic h-BN (structure is shown in Fig. 1.1) can reach up to about 300W/mK at room temperature. They also found that phonon dislocation scattering and phonon boundary scattering limit the low-temperature thermal conductivity. Interestingly, they also reported a 0.3^o rotational misalignment between neighboring crystallites, and this could affect thermal conductivity since the corresponding strain would trigger the formation of dislocation boundaries.

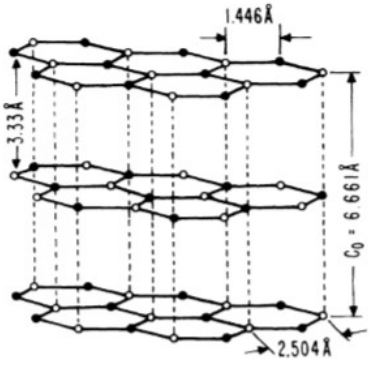

Figure 1.1: AA-stacking of h-BN [3].

Zhou et al [4] grew suspended few-layer h-BN sheets (monolayer, bilayer and nine-layer) and measured their thermal conductivity by micro-Raman spectroscopy method. The thermal conductivity is calculated from:

$$K = \chi(\frac{1}{2\pi h})(\frac{\partial w}{\partial P})^{-1}(\frac{\partial P_{h-BN}}{\partial P}) \quad (1.1)$$

Where χ is an experimental parameter which is determined by linear fitting of Raman shifts:

$$\omega - \omega_0 = \chi T \quad (1.2)$$

h is the thickness of h-BN samples, and ω denotes the peak frequency shift of Raman E_{2g} mode. $P_{h\text{-}BN}$ is the absorbed laser power by the suspended h-BN film, while P is the external laser power. It turned out that the thermal conductivity of these samples is in the range from 227 to 280 W/mK.

A recent study by Q. Cai et al [5] reported that monolayer h-BN with a high thermal conductivity which is successfully obtained by exfoliating it from h-BN single crystal, and the thermal conductivity is measured by Raman spectroscopy. The in-plane thermal conductivity of suspended h-BN could be estimated as follows:

$$\kappa = \frac{ln(\frac{R}{r_0})}{2\pi d\frac{T_m - T_a}{Q - Q_{air}}}\alpha \quad (1.3)$$

In this equation, α is the Gaussian profile factor of the laser beam, T_m is the measured Raman temperature, T_a is ambient temperature and $Q - Q_{air}$ is the absorbed heat. They concluded that thermal conductivity of 751 W/mK, while the thermal conductivity of 2-layer and 3-layer h-BN decreases to 646 W/mK and 602 W/mK.

1.2.2 Theoretical studies on h-BN monolayer systems

Often referred to as “white graphene”, h-BN is known for its outstanding physical properties, and have triggered broad interest in designing future nanoscale devices. As the development of

computational science, materials simulation based on accurate algorithms started to play an important part in modern research. While valid experimental results are the basis of constructing persuasive force field models, these force field models also provide reasonable predictions and shed light on future experimental work fields.

It is known that in pristine crystalline materials, the lattice thermal conductivity is determined by phonon-based thermal transport process. A common approach is to apply the phonon Boltzmann transport equation (BTE) to determine the thermal conductivity. L. Lindsay et al [6] provide the general expression for phonon transport in the frame of Boltzmann transport equations (BTE) for a single layer h-BN as:

$$\kappa_L = \frac{1}{4\pi^2 N\delta}\sum_j \int \left(\frac{\partial n_\lambda^0}{\partial T}\right)\frac{h}{2\pi}\omega_\lambda v_{\lambda x}^2 \tau_\lambda dq \tag{1.4}$$

In this equation, n_λ^0 denotes Bose-Einstein distribution; $v_{\lambda x} = d\omega_\lambda/dq_x$ shows the phonon group velocity along the heat transport direction; δ is the interatomic spacing of h-BN; ω_λ is the frequency of phonon mode $\lambda = (q, j)$ in which q denotes the in-plane wavevector while j denotes the phonon branch index. In their study they used a Tersoff type force field, and have fitted a set of Tersoff force field parameters. According to their calculation, the thermal conductivity of single-layer isotopically pure h-BN is about 800 W/mK at room temperature. They also studied the effect of isotope on monolayer h-BN. Isotope defects hinder thermal conductivity, and the effect depend sensitively on model size.

It is also worth noticing that the theoretical model for h-BN should be analogous to graphene due to their congruity in lattice structure. According to D. L. Nika et al [7], as the phonon wave factor q increases, Umklapp scattering starts to dominate the thermal transport process by limiting the flux of higher energy phonons. But on low-energy phonons (small-q region), other phonon-

scattering mechanisms, for example, edge roughness scattering starts to take effect. Jacimovski et al [8] provided a deduction based on BTE to calculate the lattice thermal conductivity of graphene:

$$\frac{\partial n_s(\vec{q})}{\partial t} + v \cdot \frac{\partial n_s(\vec{q})}{\partial x} = \frac{\partial n_{sc}(\vec{q})}{\partial t} \tag{1.5}$$

Here n_s denotes the phonon distribution function of vibration modes, while n_{sc} represents the collision integral. The Umklapp process and heat flux could be described as:

$$\sum_i \overrightarrow{q_i} = \vec{b} + \sum_i \overrightarrow{q_i}' \qquad \overrightarrow{W_\alpha} = -\sum_\beta \kappa_{\alpha\beta} \frac{\partial T}{\partial \chi_\beta} V \tag{1.6}$$

By considering stationary-state phonon transport, and treating the collision integral as a linear function near the equilibrium distribution, finally a general expression of lattice thermal conductivity (averaged over all orientations) could be obtained:

$$\kappa = \frac{1}{4\pi l_z k_B T^2} \sum_s \int_{\omega_{min}}^{\omega_{max}} (\hbar\omega_s)^2 \frac{e^x}{(e^x-1)^2} \tau(\omega_s) \frac{v}{u} \omega_s d\omega_s \,, \quad x = \frac{\hbar\omega_s}{k_B T} \tag{1.7}$$

Where $l_z = 3.35\dot{A}$, $\vec{v}, \vec{u}$ is group and phase velocities, $\tau(\omega_s)$ is phonon relaxation time, and can be calculated from the sum of inverse relaxation times due to different sources:

$$\frac{1}{\tau(\omega_s)} = \frac{1}{\tau_{umklapp}} + \frac{1}{\tau_{boundary}} + \frac{1}{\tau_{isotope}} + \cdots \tag{1.8}$$

Another interesting fact is that the phonon density of state (DOS) could also be calculated by doing a Fourier transformation to the velocity auto-correlation functions (VACF), as presented by J. M. Dickey et al [9]. They simplified the lattice vibration to harmonic oscillators. Let f(w) denotes the number of oscillators with frequency ω, normalization gives us that

$$\int f(w) dw = N \tag{1.9}$$

And for one oscillator, we have $x = Acos(wt + \varphi)$, $v = -Awsin(wt + \varphi)$.

For classical oscillator, we know that $m\frac{A^2\omega^2}{2} = k_B T$.

Define velocity correlation function $\gamma(t)$:

$$\gamma(t) = \frac{<\vec{v}(t)\cdot\vec{v}(0)>}{<\vec{v}(0)\cdot\vec{v}(0)>} = \frac{<\sum \sin(wt+\varphi)sin\varphi>}{<\sum si\ ^2\varphi>} \tag{1.10}$$

Averaging over random phase φ gives us that:

$$\gamma(t) = N^{-1}\sum coswt = \int f(w)\cdot coswtdt \tag{1.11}$$

The equation above showed that under classic harmonic approximation, Fourier transform of $\gamma(t)$ gives us f(w) directly.

A. Kınacı et al [10] studied the thermal conductivity of BN–C structures. They parameterized Tersoff potential among all types of interactions among B, N, C atoms, which is implemented as a potential file in LAMMPS, and they also systematically studied different types of BN-C hybrid grain boundary structures. Based on this set of Tersoff interaction parameters, the thermal conductivity of BN structures was also studied by C. Sevik et al [11]. The thermal conductivity of monolayer defect-free h-BN is reported to be about 400 W/mK at room temperature. They also gave the temperature dependence curve of h-BN and its comparison to graphene of the same size and boundary shape, as shown in Fig. 1.2 and Tab. 1.2:

$A = 1433.0$ eV	$B = 417.30$ eV		A (eV)	1380	B (eV)	340.0
$\lambda_1 = 3.4661$ Å^{-1}	$\lambda_2 = 2.2288$ Å^{-1}		λ_1 (Å^{-1})	3.568	λ_2 (Å^{-1})	2.199
$\lambda_3 = 0.0000$ Å^{-1}	$n = 0.72674$		λ_3 (Å^{-1})	0.000	n	0.727 51
$c = 30692.4$	$\beta = 1.0239 \times 10^{-7}$		c	25 000	β (10^{-7})	1.257 24
$d = 4.7295$	$h = -0.98578$		d	4.3484	h	−0.890 00
$R = 1.95$ Å	$D = 0.15$ Å		R (Å)	1.950	D (Å)	0.050
$\varepsilon = 0.004$ eV	$\sigma = 0.3212$ nm					

Table 1.1: A comparison of Tersoff parameters for B-N interactions. The left part is parameter fitted in [6] (ε and σ is LJ parameter here), while the right part is parameter fitted in [10,11].

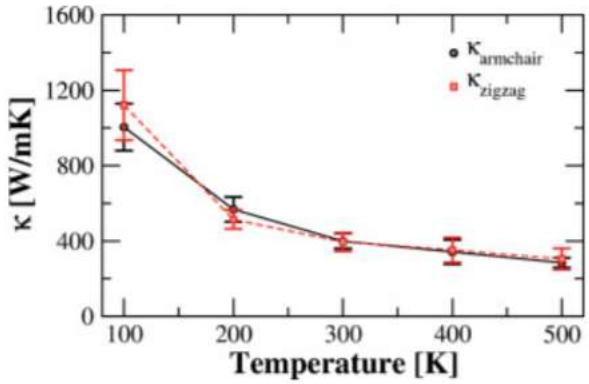

Figure 1.2: Temperature dependence of thermal conductivity of h-BN nanoribbon along zigzag/armchair direction [11].

Structure	κ (W/mK)	Structure	κ (W/mK)
Graphene	2500	BNWG	400
z-GNR(~12 nm)	1700	z-BNNR(~12 nm)	350
z-GNR(~20 nm)	2300	z-BNNR(~20 nm)	380
a-GNR(~12 nm)	1025	a-BNNR(~12 nm)	260
a-GNR(~20 nm)	1859	a-BNNR(~20 nm)	360
CNT(10,0)	955	BNNT(10,0)	430
CNT(10,10)	940	BNNT(10,10)	465

Table 1.2: A comparison of h-BN nanoribbon and graphene nanoribbon along zigzag (z-) and armchair (a-) direction at T=300K [11].

There are other forms of atomic interactions proposed by researchers. For instance, J. H. Los et al [12] developed a new set of equations and corresponding parameters for "Extended Tersoff Potential" and proved that this potential could fit the elastic properties of both pristine and defective h-BN systems well. T. Maaravi et al [13] improved the former-proposed KC-ILP model, taking Coulombic term into consideration to better simulate the interlayer interactions of graphene and h-BN. However, most of the published theoretical simulations still adopted Tersoff potential with first two set of parameters for in-plane atomic interactions. And although LJ potential may not be the most proper description for interlayer interactions, they still proved to be concise, efficient and with tolerable accuracy, thus still widely applied in MD simulations.

In practice, the existence of defects, including the formation of dislocations, vacancies and grain boundaries, is inevitable. Y. Liu et al [14] constructed different grain boundaries in 2-D h-BN monolayer and calculated the grain boundary energy. They proposed that there may also exist square-octagon pairs so that formation of energetically unfavorable N-N and B-B bonds could be avoided. According to their report, square-octagon (4|8) structures are energetically favorable than pentagon-heptagon (5|7) structures, but may also cause larger out-of-plane convex. Fig. 1.3 presented a possible formation path of such structure when two 5|7 grain boundaries are adjacent to each other:

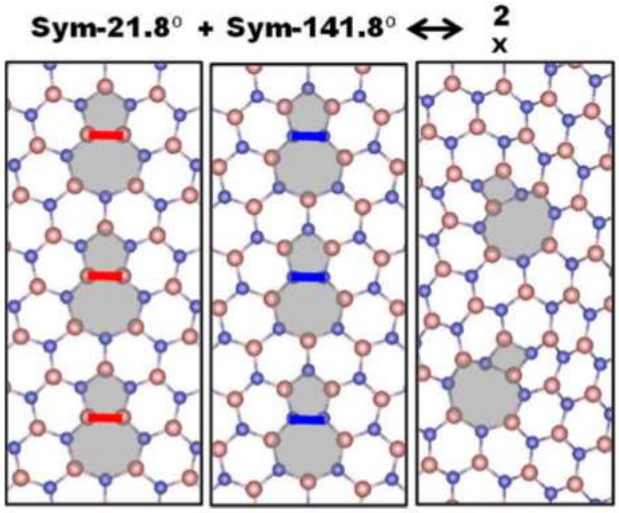

Figure 1.3: One possible transformation "reaction" from 5|7 to 4|8 structures [14].

Heptagon-pentagon grain boundaries could be constructed by tilting two neighboring nanosheets to different orients. The misorientation angle could be represented as:

$$\theta = \theta_l + \theta_r$$

$$\theta_{l,r} = tan^{-1}\left(\frac{\sqrt{3}m_{l,r}}{m_{l,r}+2n_{l,r}}\right) \tag{1.12}$$

$$L_p = |n\vec{a}_1 + m\vec{a}_2| = a_0\sqrt{n^2 + mn + m^2}\,, \qquad |a_{0,1,2}| = 2.46\dot{A}$$

According to equation (1.5), symmetric/asymmetric grain boundaries can be constructed depending on whether the rotational axis points along zigzag or armchair direction. Timon Rabczuk et al [15] calculated the thermal conductivity of pristine h-BN and graphene nanoribbons with direct NEMD method. Their simulation sample had 660nm in length and was divided into 20 areas with different temperature. Reactive empirical bond order (REBO) potential was applied, and the temperature gradient is shown in Fig. 1.4:

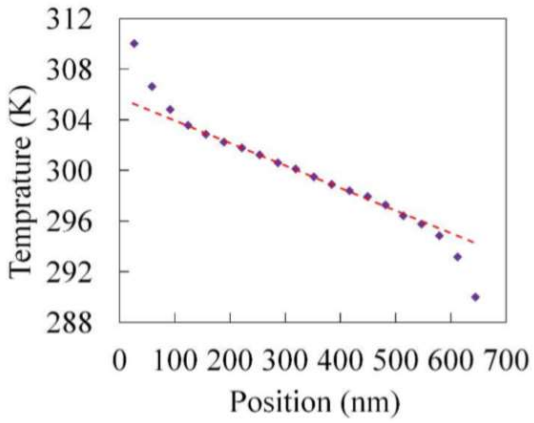

Figure 1.4: The temperature gradient exerted to 660nm length in case [15].

	Thermal Conductivity (W/m·K)		
	300 Kelvin	**500 Kelvin**	**700 Kelvin**
h-BN	606.58	400.26	359.54
Graphene	2941.18	1596.17	1048.22

Table 1.3: The thermal conductivity calculated by NEMD method [15].

A research by A. Tabarraei [16] treated the thermal conductivity of monolayer boron nitride nanoribbons by reverse non-equilibrium molecular dynamics method (will be introduced in next chapter). The thermal conductivity of 2.4 nm wide h-BN nanoribbon pointing along both zigzag and armchair direction is reported to increase as its length increases to 250 nm. Zigzag h-BN

nanoribbons tend to have larger thermal conductivity than armchair h-BN nanoribbons of the same length. Interestingly, compared with nanoribbon length, the width of simulation samples does not have much influence on calculated thermal conductivity. Samples of length 11 nm with a width range from 1 nm to 11 nm showed a minor decrease of about 20% for both zigzag and armchair ribbons.

It is also worth noticing that in realistic crystal growth process, polycrystalline single-layered h-BN is likely to appear due to multiple crystalline nucleus. B. Mortazavi et al [17] applied EMD method and finite element analysis to simulate the thermal conductivity of polycrystalline h-BN monolayer. According to their result, the thermal conductivities of polycrystalline h-BN at T=300K is about 1/3 of the pristine monocrystalline nanosheet. However, more studies concerning polycrystalline h-BN is needed before any consensus could be reached.

2. COMPUTATIONAL METHODOLOGY

Computer simulations act as linkers between materials properties in microscopic size and timescales, and macroscopic properties measured in the laboratory. In general, microscopic algorithms can be classified as Molecular dynamics (MD) and Monte Carlo (MC) methods. In this study, we will only discuss MD approaches.

MD simulation consists of the numerical iterative solution of the Newtonian dynamic equations of motion. In this n-body system, the equations of motion for an atom indexed i is given by:

$$m_i \ddot{r}_i = f_i \qquad f_i = -\frac{\partial}{\partial r_i} U(r^N) \tag{2.1}$$

where U(r^N) is typically referred to as the force field of the system, and r^N denotes a set of 3N atomic coordinates. For simplicity, interactions higher than 3-body terms are not taken into consideration in the following discussion.

2.1. Non-bonded Interactions

Generally, force field contains both bonded and non-bonded interactions. Non-bonded interactions act between atoms in the same molecule and those in other molecules. There are two major classes of non-bonded interactions: electrostatic interaction and Van der Waals interaction.

The general expression of non-bonded interactions can be described as:

$$U_{non-bonde}\ (r^N) = \sum_i V(r_i) + \sum_{j>i} V(r_i, r_j) + \sum_{i<j<k} V(r_i, r_j, r_k) + \cdots \tag{2.2}$$

The V(r) term represents an externally applied potential field or the effects of the container walls; it is usually dropped for fully periodic simulations of bulk systems. Sometimes it is also possible to concentrate on the pair potential $V(r_i, r_j) = V(r_{ij})$ instead of considering higher order interactions.

The most widely known non-bonding interactions are probably Leonard-Jones interaction and electrostatic Coulombic interaction. They have been widely applied to fields of classic and semi-classic materials modeling. However, in most cases the result of simulation considering only 2-body potentials would be insufficient to represent the full physics of the material. Thus, multi-body interactions are developed theoretically and applied in computer simulations. Some widely applied multi-body interactions includes Embedded atom model (EAM), Reactive empirical bond-order (REBO) potential, Tersoff bond order dependent potentials, etc.

In an MD simulation, computing of the non-bonding interactions often involves a large number of pairwise calculations. For example, the time to examine all pair separations in an N-atom system is proportional to the number of distinct pairs, $\frac{1}{2}N(N-1)$. To avoid expensive calculations, the concept of neighbor list is introduced into computing algorithms. Verlet proposed a classic technique: all pairs of interaction are calculated every n step at the beginning, and for a given atom i, a table of surrounding atoms j that satisfy condition $r_{ij} < r_c$ are constructed at the same time. Errors would be eliminated when r_c is sufficiently larger than r_{ij} so that no particle outside the table traverses the distance of $r_c - r_{ij}$ and gets into the range of the potential [18]. The neighbor list could be shown as posted below:

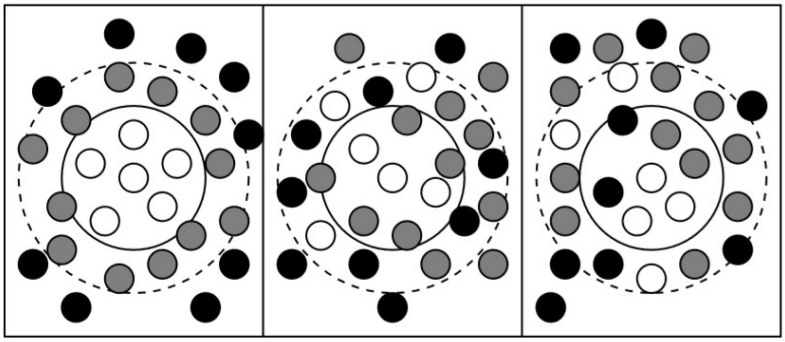

Figure 2.1: The Verlet list on its construction, later, and too late [19]. The potential cutoff range is denoted in solid circle, while the list range is denoted in dashed circle.

As it could be observed, a new neighbor list must be constructed before particles originally outside the list range (denoted as the darkest dots) have penetrated the potential cutoff sphere.

2.2. Numerical Algorithms: Verlet Algorithm

In molecular dynamics, the most commonly used time integration algorithm is probably the so-called Verlet algorithm. The basis of this iteration method is to obtain the Taylor expansion of position r. Given v as the velocities, a as the accelerations, and b to be the third derivatives of r with respect to t, one has:

$$r(t+\Delta t) = r(t) + v(t)\Delta t + \frac{1}{2}a(t)\Delta t^2 + \frac{1}{6}b(t)\Delta t^3 + O(\Delta t^4)$$

$$r(t-\Delta t) = r(t) - v(t)\Delta t + \tfrac{1}{2}a(t)\Delta t^2 - \tfrac{1}{6}b(t)\Delta t^3 + O(\Delta t^4) \quad (2.4)$$

Adding up the two equations above gives us:

$$r(t+\Delta t) = 2r(t) - r(t-\Delta t) + a(t)\Delta t^2 + O(\Delta t^4) \quad (2.5)$$

And Newton's laws give us:

$$a(t) = -\tfrac{1}{m}\nabla V(r(t)) \quad (2.6)$$

It is obvious that the truncation error of the algorithm when evolving the system by is of the order of Δt^4, the third derivatives do not appear explicitly, cancelled upon summing the two. This guaranteed the accuracy of this algorithm. In the meantime, this algorithm is also stable and simple to implement.

However, a problem with this version of the Verlet algorithm is that velocities are not directly generated. While they are not needed for the time evolution, their knowledge is sometimes necessary. For example, the calculation of phonon density of state or calculation of viscosity always needs velocity autocorrelation functions. Moreover, they are required to compute the

kinetic energy K, whose evaluation is necessary to test the conservation of the total energy E=K+V. This is one of the most important tests to verify that a MD simulation is proceeding correctly. One could compute the velocities from the positions by:

$$v(t) = \frac{r(t+\Delta t) - r(t-\Delta t)}{2\Delta t} \tag{2.7}$$

And it is easy to find that the error of v(t) is at the order of Δt^2, more significant than Δt^4. To overcome this difficulty, some variants of the Verlet algorithm have been developed. They give rise to exactly the same trajectory, and differ in what variables are stored in memory and at what times. Among them the most representative one is the velocity Verlet algorithm.

A different form of Verlet algorithm, the velocity Verlet algorithm uses velocities explicitly. Positions, velocities and accelerations at time $t + \Delta t$ are obtained from the same quantities at time t in the following way:

$$r(t + \Delta t) = r(t) + v(t)\Delta t + \frac{1}{2}a(t)\Delta t^2$$

$$v\left(t + \frac{1}{2}\Delta t\right) = v(t) + \frac{1}{2}a(t)\Delta t$$

$$a(t + \Delta t) = -\frac{1}{m}\nabla \mathrm{V}(\mathrm{r}(\mathrm{t} + \Delta \mathrm{t}))$$

$$v(t + \Delta t) = v\left(t + \tfrac{1}{2}\Delta t\right) + \tfrac{1}{2}a(t + \Delta t)\Delta t + O(2) \tag{2.8}$$

In these expressions, v is the velocity, a is the acceleration, and O(N) asserts a numerical error of order N. The time step, Δt, must be sufficiently small to allow numerical stability; usually this is similar to the characteristic timescale of atomic vibrations, $\sim 10^{-15}$ s. The formulas in Eq. 2.8 are then iterated a number of times, n, to produce atomic motion for a desired period, nΔt.

2.3. Equilibrium versus Non-equilibrium Molecular Dynamics

As the mechanics of MD have been generally described, how the atomic velocities relate to the thermodynamic state of the system, and how they lead to the determination of thermodynamic properties are discussed in this section. Atomic velocities are randomly chosen at the beginning of an MD simulation such that the total momentum of the system is zero. By scaling the velocities, a macroscopic value of temperature is calculated according to its thermodynamic connection to kinetic energy:

$$\frac{3}{2}Nk_BT = \frac{1}{2}\sum_i m_i {v_i}^2 \tag{2.9}$$

Throughout this work, the simulation is constrained to have a fixed number of atoms N and a constant volume V. All the simulation systems are relaxed in Noose-Hoover heat bath. All the thermal data is measured under microcanonical ensemble (NVE) due to the adiabatic nature of the simulation system.

In statistical physics, we know that the ensemble average of certain thermodynamic property B in a microcanonical system is given by:

$$\langle B_{NVE} \rangle = \frac{1}{\Omega}\int_{\Gamma} B(v(t), r(t))dvdr \tag{2.10}$$

where Ω is the partition function of the system, the total number of states in NVE, and Γ denotes all the possible values of r and v in the phase space (Γ = {r,v}). Generally speaking, this expression is valid only if the time duration of the simulation is long enough to allow the system to reach to all possible states in its {r,v} phase space, thus satisfying the ergodic hypothesis: over a long period of time, all accessible microstates are eventually equiprobable. For simulations considered in this work, a sufficient time is often on the order of nanoseconds.

2.3.1. Equilibrium molecular dynamics (EMD) approaches

EMD approach often provides a constant distribution of properties, for instance, temperature or pressure, across certain simulation system. The physical properties rendered through this kind of simulation are based on the linear response theory of certain related "random force" in a given system, where the fluctuation-dissipation theorem plays an important part. This theorem relates transport coefficients to the ensemble average of corresponding auto-correlation functions. R. Kubo [20] derived this formula by applying linear response theory to Brownian dynamics in order to describe the intrinsic relation between statistical auto-correlation and physical particle actions. For the EMD simulations in this work, we will only apply a particular category of time-correlations known as autocorrelation functions (ACF). For a given property calculated through molecular dynamics, the autocorrelation function takes the form below:

$$C(t) = \frac{1}{N}\sum_{i=0}^{N} A(t+\tau_i)\,A(\tau_i) = < A(t)A(0) > \tag{2.11}$$

Moreover, the inner relation between thermal conductivity and other thermodynamic properties, could be deduced by the generalized Langevin equation for Brownian motion, as well as basic diffusion theory [21]. Generally, we will refer to the equation:

$$\frac{dA(t)}{dt} = -\int_0^t K(t-t')A(t')dt' + F(t) \tag{2.12}$$

in which A(t) is the phase variable, K(t) is the time dependent transport coefficient, F(t) is the random force. Assuming that the equilibrium canonical ensemble average of the random force and the phase variable eventually decrease to zero:

$$\langle A(0)\cdot F(t)\rangle = \langle A(t_0)\cdot F(t_0+t)\rangle = 0 \tag{2.13}$$

The time displacement by t_0 is allowed because the equilibrium time correlation function is independent of the time origin. By multiplying the complex conjugate of A(0) for both sides of the

equation above and then taking a canonical average, we have a new function C(t) defined to be the equilibrium autocorrelation function $C(t) = \langle A(t) \cdot A^*(0) \rangle$, and we could see that

$$\frac{dC(t)}{dt} = -\int_0^t dt' K(t-t') C(t') \tag{2.14}$$

Taking the Laplace transform gives us that

$$\int_0^\infty dt\, e^{-st} \frac{dC(t)}{dt} = s\tilde{C}(s) - C(0) \tag{2.15}$$

And the right side of equation (2.14) becomes Laplacian transform convolution. Namely, we have

$$s\tilde{C}(s) - C(0) = -\widetilde{K}(s)\tilde{C}(s) \tag{2.16}$$

Noticing that mathematically, the double differentiation of C(t) could be presented as:

$$\frac{d^2}{dt^2} C(t) = -\varphi(t) = \langle \dot{A}(t) \cdot \dot{A}^*(0) \rangle \tag{2.17}$$

Taking the Laplace transform of $\varphi(t)$ will give us that:

$$-\tilde{\varphi}(s) = s^2\tilde{C}(s) - sC(0) \tag{2.18}$$

And eliminating $\tilde{C}(s)$ with the two equations above gives us that:

$$\widetilde{K}(s) = \frac{\tilde{\varphi}(s)}{C(0) - \tilde{\varphi}(s)/s} \tag{2.19}$$

By repeating similar process for thermal conductivity calculation, we could have

$$\tilde{C}(k, \omega) = \frac{C(k,0)}{i\omega + k^2 D(k,\omega)} \tag{2.20}$$

Where C(t) is the energy correlation function, and $\tilde{C}(k, \omega)$ denotes the Fourier-Laplace transform of given C(t):

$$\int_0^\infty C(t) e^{-i\omega t} dt = \tilde{C}(\omega) \tag{2.21}$$

And correspondingly, we have $\varphi(k,t) = k^2 \langle J(-k,0) \cdot J(k,t) \rangle$. It is worth noticing that the Green-Kubo relations are only valid for infinitely slow processes. To render the correct expression in Green-Kubo form, we must take the zero wavevector k limit and zero frequency w limit since relaxation process is only infinitely slow at zero wavevector.

Finally, according to the Green–Kubo theory, the thermal conductivity tensor is proportional to the time integral of the heat current autocorrelation function (HCACF). For thermal conductivity calculations, the Green-Kubo formula takes such form [22]:

$$\kappa_{ij} = \frac{1}{Vk_BT^2} \cdot \int_0^\infty < J_i(0) J_j(t) > dt$$

$$\mathrm{J} = \sum_{i=1}^{N} \varepsilon_i v_i + \frac{1}{2} \sum_{i \neq j} r_{ji} (f_{ij}^i \cdot v_i) \tag{2.22}$$

where T is the temperature, k_B is the Boltzmann constant, V is the domain volume, $J_i(t)$ is the time-dependent heat current along the i-th (i = x, y, z) direction, and <·> represents the ensemble average. f_{ij} is the force on atom i exerted by its neighboring atom j, r_{ji} is the distance vector pointing from atom j to atom i. Given U_{ij} the atomic force field, atomic energy of atom i, ε_i, is expressed by:

$$\varepsilon_i = \frac{1}{2} m_i {v_i}^2 + \frac{1}{2} \sum_{i \neq j} U_{ij} \tag{2.23}$$

2.3.2. Non-equilibrium molecular dynamics (NEMD) approaches

NEMD methods tend to calculate the thermal conductivity directly through imposing a direct temperature gradient. The simplest method is to set a temperature gradient to certain simulation system. During the simulation period, the corresponding heat flux density data is recorded, and thermal conductivity, κ, could be obtained by directly applying Fourier's law:

$$\mathrm{J} = -\kappa \cdot \nabla \mathrm{T} \tag{2.24}$$

where J is the steady-state heat flux and ∇T is the temperature drop across the heat flowing direction. The thermal conductivity of certain material along the heat flux direction (e.g. the x-direction) was calculated by:

$$\kappa(L) = \frac{J}{dT/dx} \tag{2.25}$$

The calculated κ is shown as a function of L (model length along the heat flux direction), because NEMD results are known to have prominent length effects. Based on many previous studies, this length effect is dealt by an empirical equation:

$$\frac{1}{\kappa(L)} = \frac{1}{\kappa_0}\left(\frac{\lambda}{L} + 1\right) \tag{2.26}$$

where κ_0 is the thermal conductivity at the infinite length (so that the length effect does not play a role), and λ is the phonon mean free path.

NEMD methods usually give us a straightforward value of κ in the heat flux transport direction. It is worth noticing though, since the temperature gradient could be unphysically large (about $10^8 K/m$), the local stability of our model may not be guaranteed, thus the systematic error could be relatively large if the size of our model is not large enough.

Florian Muller-Plathe [23] first proposed an alternative non-equilibrium method to calculate thermal conductivity. Instead of imposing high temperature and low temperature regions to create temperature gradient, he proposed that given z the heat transfer direction, thermal conductivity can be calculated as:

$$\kappa = \lim_{\partial T/\partial z \to 0} \lim_{t \to \infty} -\frac{<J_z(t)>}{<\partial T/\quad>} \tag{2.27}$$

He then divided the periodic simulation box into N slabs. Slab 0 is "cool slab", while slab N/2 is "hot slab". Thus, the instant kinetic temperature of each slab can be calculated as follows:

$$T_k = \frac{1}{3 n_k k_B} \sum_{i \in k}^{n_k} m_i {v_i}^2 \tag{2.28}$$

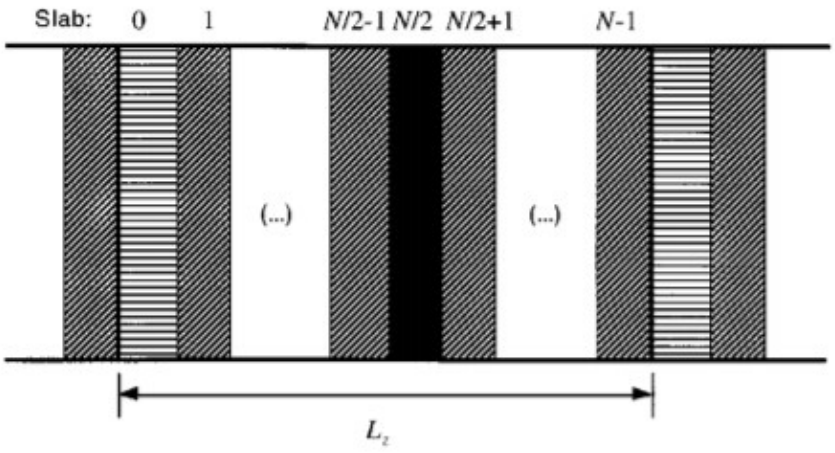

Figure 2.2: Subdividing the periodic simulation box to N slabs for heat transfer calculation [23].

The heat flux is generated by exchanging the velocity vectors of atoms in the cool slab and the same number of atoms in the hot slab so that the temperature increases in the hot slab and decreases in the cool slab. In this way, the total energy of simulation system remains the same. For simulation samples with orthogonal periodicity, given the truncation area $S = L_x L_y$, total simulation time t, and the subscript h, c refers to the hot and the cold particle. Mind that the masses of velocity-interchanging particles should be the same. In this case, we will have the expression of thermal conductivity as:

$$\lambda = -\frac{\sum_{transfers}\frac{m}{2}(v_h{}^2 - v_c{}^2)}{2tL_xL_y\langle \partial T/\partial z\rangle} \tag{2.29}$$

2.4. Simulation Methodology Applied in This Work

To calculate in-plane and interlayer thermal conductivity, one must specify the interatomic potential. In this research, LJ potential is applied to simulate all the interlayer atomic interactions, with parameters specified are taken from universal force field (UFF) [24], while Tersoff potential is applied for in-plane atomic interactions.

For LJ potential, the UFF gives the potential in the form of:

$$E_{vdw} = D_{IJ}\left\{-2[\frac{x_{IJ}}{x}]^6 + [\frac{x_{IJ}}{x}]^{12}\right\}$$

$$r_{IJ} = r_I + r_J + r_{BO} + r_{EN}, \quad x_{IJ} = \frac{1}{2}\left(x_I + x_J\right), \quad D_{IJ} = (D_I D_J)^{\frac{1}{2}} \tag{2.30}$$

Where r_{IJ}(the natural bond length) is assumed to be the sum of atom type specific single bond radii, a bond order correction and an electronegativity correction. x_I is the atomic Van der Waals distance, which is analogous to r_{IJ}. D_I is the atomic Van der Waals energy, D_{IJ} is the well depth in kcal/mol and x_{IJ} is the Van der Waals bond length in $\dot{A}$.

In LAMMPS, LJ potential is denoted as:

$$4\varepsilon\left[(\frac{\sigma}{r})^{12} - (\frac{\sigma}{r})^6\right], \quad r < r_c \tag{2.31}$$

Comparing the two equations above gives us that $D_{IJ} = 2\varepsilon$, $x_{IJ} = \sqrt[6]{2}\sigma$.

The universal force field parameters are listed below, in Tab. 2.1 [24]:

	valence		nonbond			effective
atom type	bond r_1^a	angle θ_0^b	distance x_1^a	energy D_1^c	scale ζ	charge Z_1^{*d}
H_	0.354	180.0	2.886	0.044	12.0	0.712
H_b	0.460	83.5	2.886	0.044	12.0	0.712
He4+4	0.849	90.0	2.362	0.056	15.24	0.098
Li	1.336	180.0	2.451	0.025	12.0	1.026
Be3+2	1.074	109.47	2.745	0.085	12.0	1.565
B_3	0.838	109.47	4.083	0.180	12.052	1.755
B_2	0.828	120.0	4.083	0.180	12.052	1.755
C_3	0.757	109.47	3.851	0.105	12.73	1.912
C_R	0.729	120.0	3.851	0.105	12.73	1.912
C_2	0.732	120.0	3.851	0.105	12.73	1.912
C_1	0.706	180.0	3.851	0.105	12.73	1.912
N_3	0.700	106.7	3.660	0.069	13.407	2.544
N_R	0.699	120.0	3.660	0.069	13.407	2.544
N_2	0.685	111.2	3.660	0.069	13.407	2.544
N_1	0.656	180.0	3.660	0.069	13.407	2.544

Table 2.1: Atomic data of boron and nitride in elemental form, in unit a=Angstrom, b=degree, c=kcal/mol, d=charge.

In this work, Coulombic interactions are not taken into consideration since B-N bonds are more inclined to covalent bonds judged by electronegativity value of boron (about 2.0) and nitrogen (about 3.0) atoms. The short-range (LJ) terms were truncated at 16 Å. Periodic boundary conditions were applied along all directions.

Tersoff potential is applied to simulate in-plane three-body atomic interactions of h-BN structures in this work. This potential is first defined by Tersoff [25] as:

$$E = \sum E_i = \frac{1}{2}\sum_{i \neq j} V_{ij}$$

$$V_{ij} = f_c(r_{ij})[f_R(r_{ij}) + b_{ij} f_A(r_{ij})]$$

$$f_c(r) = \begin{cases} 1 \\ \frac{1}{2} - \frac{1}{2}\sin\left(\frac{r_{ij} - R_{ij}}{D}\pi\right), & R - D < r_{ij} < R + D \\ 0 \end{cases}$$

$$f_R = A_{ij}\exp\left(-\lambda_{ij}^{I} r_{ij}\right), \qquad f_A = -B_{ij}\chi_{ij}\exp\left(-\lambda_{ij}^{II} r_{ij}\right)$$

$$b_{ij} = \left(1 + {\beta_i}^{n_i}{\xi_{ij}}^{n_i}\right)^{-\frac{1}{2n_i}}, \qquad \xi_{ij} = \sum_{k \neq i,j} f_c\, g(\theta_{ijk})$$

$$g(\theta_{ijk}) = 1 + \frac{c_i^2}{d_i^2} - \frac{c_i^2}{[d_i^2 + (cos\theta_{ijk} - h_i)^2]} \tag{2.32}$$

The lower indices i, j marks the i-j bonding atoms, and k marks a third atom that lead to modification of pure i-j interactions [10,11,25]. For the determination of all physical parameters, we will apply the same set of fitted parameters as reported in [10,11].

3. RESULTS AND DISCUSSION

3.1 EMD Simulation for Bulk h-BN Systems

Boron nitride (BN) has different types of structural formation that relies in the lattice plan direction of boron and nitrogen atoms. The structures include amorphous, hexagonal, cubic, wurtzite form. Among the abovementioned BN structures, hexagonal boron nitride is known for various applications due to its outstanding thermal, mechanical and electrical properties along with its noteworthy chemical stability. In this section, we will give a brief discussion about the natural form of h-BN as well as the simulation results of its thermal conductivity.

The crystalline structure of bulk h-BN could be described as follows:

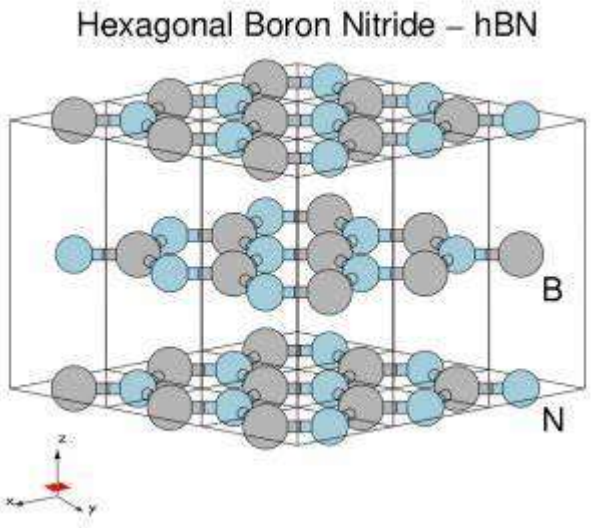

Figure 3.1: Crystalline structure of bulk h-BN

Similar to graphite, bulk hexagonal boron nitride also takes the stacking form of honeycomb layer-by-layer structure. The layers in bulk h-BN can take many stacking modes, including A-A stackings, A-B stackings (the same as graphite), A-B-C stackings, etc. In this section, we simulate the thermal properties of bulk h-BN that could exist stably in nature.

In this simulation, we applied Tersoff potential for in-plane force field simulation, while LJ potential is applied for interlayer interactions ones. A sample of 1600 atoms, with 24.6 nm in width, 42.6 nm in length, 4 atomic layers in height is studied. The system is first thermally equilibrated in NVT ensemble for 500 ps under room temperature, and then a 2 ns run under NVE ensemble is conducted to obtain reliable result of heat flux and thermal conductivity. Timestep is set to be 0.5fs.

Interestingly, during the thermal relaxation simulation, the structure of bulk h-BN changes from strict A-A stacking to A-B stacking, presenting the same morphology as graphite, as shown in Fig. 3.2. This may be result from the use of LJ potential, since it only approximately describes the interlayer atomic interactions. Unlike carbon atoms in graphite, the electronegativity of nitrogen atoms is slightly larger than that of boron atoms. Thus, the electrostatic interlayer interaction is not zero in bulk h-BN structures, we ignored the electrostatic interaction between layers.

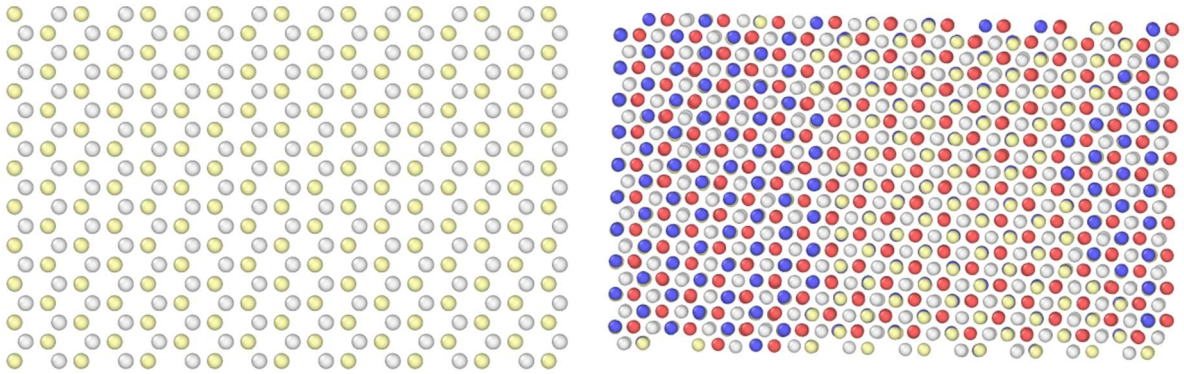

Figure 3.2: Top view of typical structure of bulk h-BN before and after thermal balancing at T = 300K. The left figure showed an A-A stacking model for bulk h-BN, while the right figure showed A-B stacking after NVT ensemble relaxation. (red and wight dots denote B atoms, while yellow and blue ones denote N atoms).

Reliable thermal conductivity calculations via EMD require the system to reach to the equilibrium, which can be characterized by the HCACF. The raw data of heat current autocorrelation function (HCACF) for such a multilayer system is plotted in Fig. 3.3. HCACF decreases drastically in about 0.5 ps, and then it starts to vibrate near the original position (HCACF

= 0). The vibration of HCACF corresponds to the vibration of atoms near its balanced position. This is typical behavior of heat transfer mechanism in bulk solid [26]. Previous EMD studies on other materials have demonstrated two different kinds of decay of the HCACF: for materials such as silicon and solid argon, the HCACF usually showed monotonous decay in the positive quadrant, while for materials such as quartz, large oscillations of HCACF are found between the positive and negative quadrants as the absolute value decays. Our result showed that bulk h-BN falls into the second category [27].

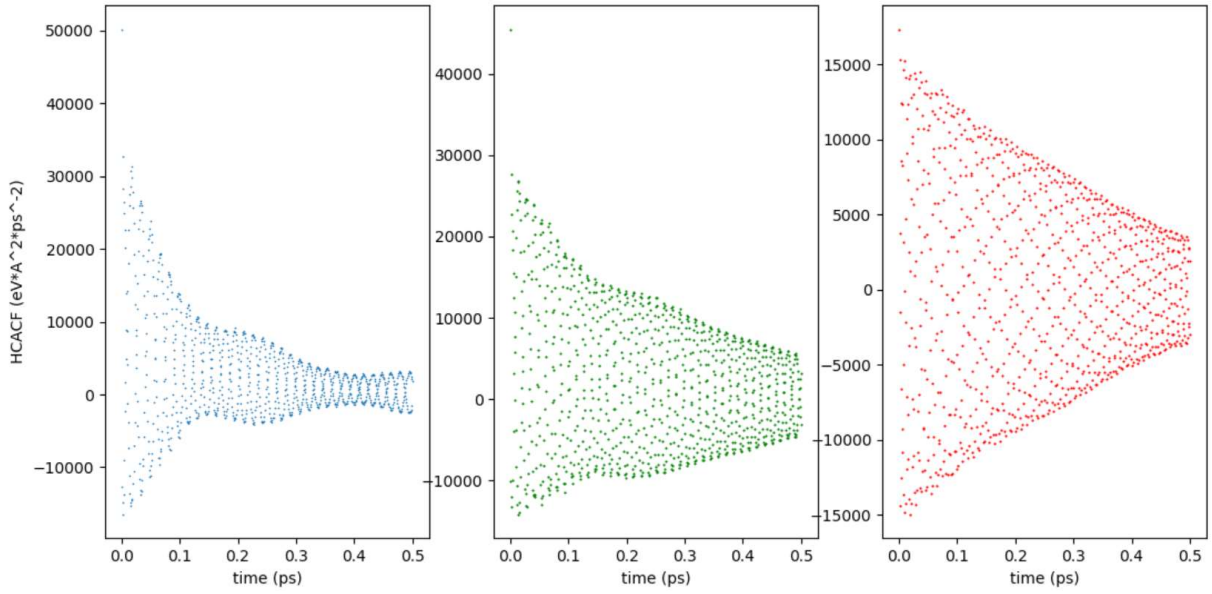

Fig. 3.3(a)

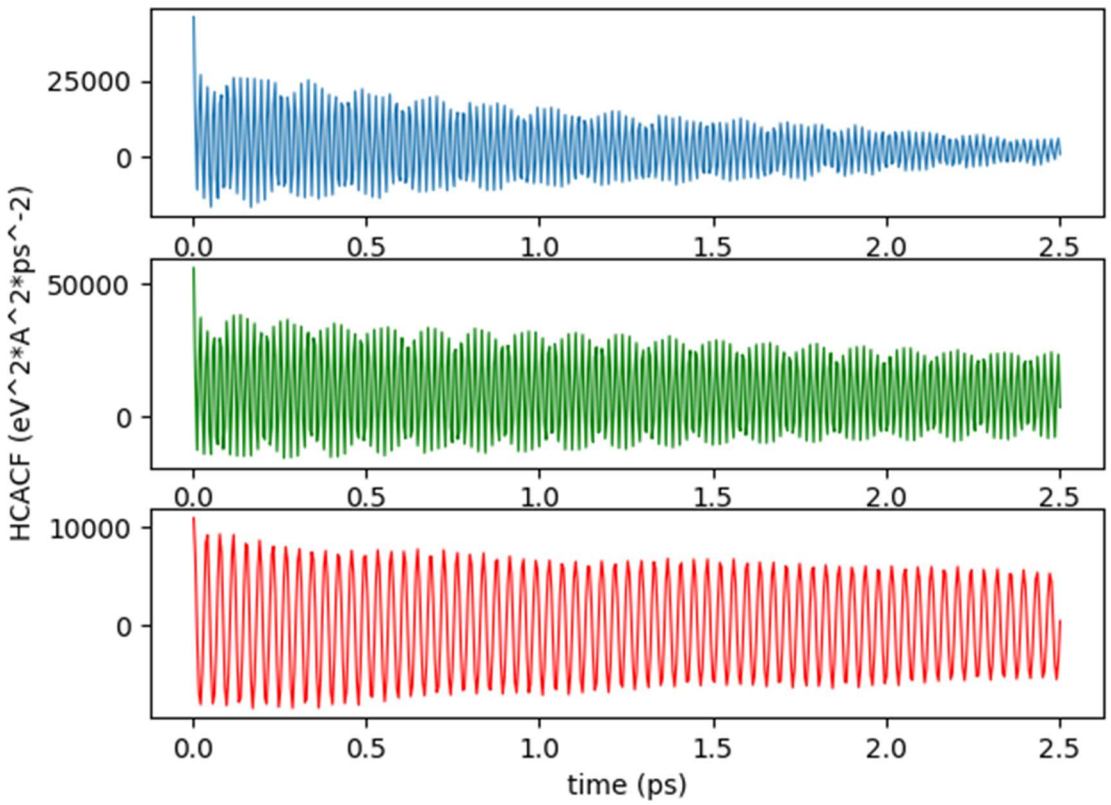

Fig. 3.3(b)

Figure 3.3: The heat current auto-correlation function of multilayer system. The HCACF profile for the bulk system is measured at 300 K. Blue/green/red dot denotes the calculated value of auto-correlation function in x/y/z axis, respectively. (a). Whole set of raw data at the beginning 0.5 ps are shown despite the total correlation time of 50 ps. (b). To better show the oscillation of HCACF, <J(t)J(t+dt)> data are calculated every 10 timesteps (dt = 5fs).

Since in all three heat transfer directions, the HCACF profiles decay rapidly within the first couple of picoseconds, a correlation length of 50 ps in this case could give a converged value of thermal conductivity tensor. The obtained in-plane thermal conductivity value is $\kappa_{xx} = 173.9 W/mK$, $\kappa_{yy} = 180.0 W/mK$, and out-of-plane thermal conductivity $\kappa_{zz} = 5.3 W/mK$, which fell in the range of experimental measured data of bulk h-BN (150 to 225W/mK) [1].

3.2 For h-BN Monolayer: A Comparison Between EMD and NEMD Method

3.2.1 Applying EMD method

Low-dimensional systems, such as MoS_2, graphene and h-BN usually exhibit superior physical properties. Hexagonal boron nitride monolayer shared the same honeycomb structure as graphene. The development of modern CVD techniques leading to defect-free 2-D structures in the order of μm makes it possible for these materials to truly render contribution to future device designing. Thus, pristine free-standing monolayer structures have become an attractive topic of research. In this section, the thermal conductivity of a pristine monolayer system (24.6nm in length, 17.4nm in width) with 16000 atoms in total is investigated. The simulation timestep is set to be 1fs, as reported in [21]. We first exerted a 1ns thermal balancing process, under canonical (NVT) ensemble, with temperature fixed to 300K. Then a microcanonical (NVE) ensemble is applied for thermal transport data collection and thermal conductivity calculation process, with a simulation length of 5ns. To eliminate the impact of interlayer atomic interaction, the lattice constant along z direction is selected 10 times larger than normal interlayer distance.

Fig. 3.4 showed an example of normalized data of heat current autocorrelation function along x direction (the zigzag direction) for one single calculation as well as the integral value of this data given different correlation time length. The correlation function reduces to zero in less than 10 ps. However, it could be observed from Fig. 3.4 that after convergence, there still exist small oscillations in the HCACF. Although this plot seems to show final convergence when correlation length reaches to 100 ps, it is still worth noticing that the noise makes direct integration of one single dataset less reliable for thermal conductivity calculations.

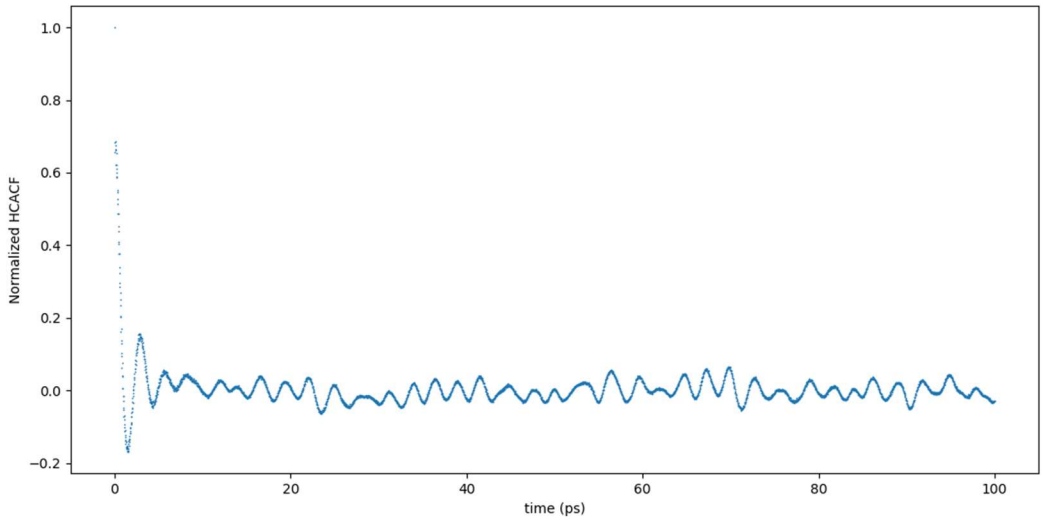

Figure 3.4: Normalized HCACF of <J(x)J(0)>/<J(0)J(0)> for an single run. Raw HCACF data are collected for only one single time period.

To avoid this problem, we smoothed the data by calculating HCACF from heat flux data. The new HCACF data for algebraic fitting could be denoted as:

$$< J(t) \cdot J(0) > |_s \; = \frac{1}{i} \sum_i < J(t_i) \cdot J(t_i + \Delta t) > \tag{3.1}$$

where different initial moments t_i were selected, while Δt remained the same. Fig. 3.5 Showed the smoothed HCACF data with i = 50 and i = 200 separately. Compared with Fig. 3.4, the tail part of HCACF data turned out to be flat, meaning the systematic noise effectively erased.

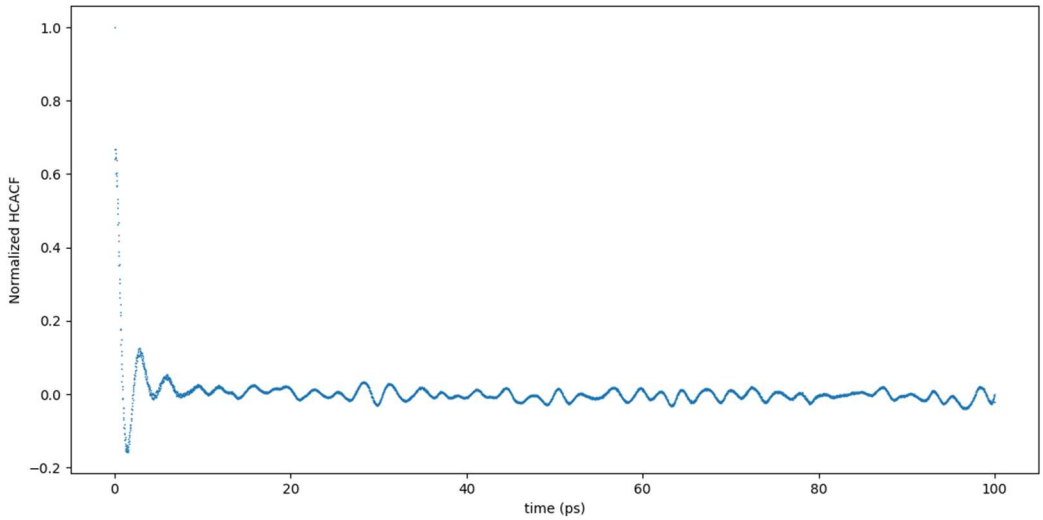

Fig. 3.5(a)

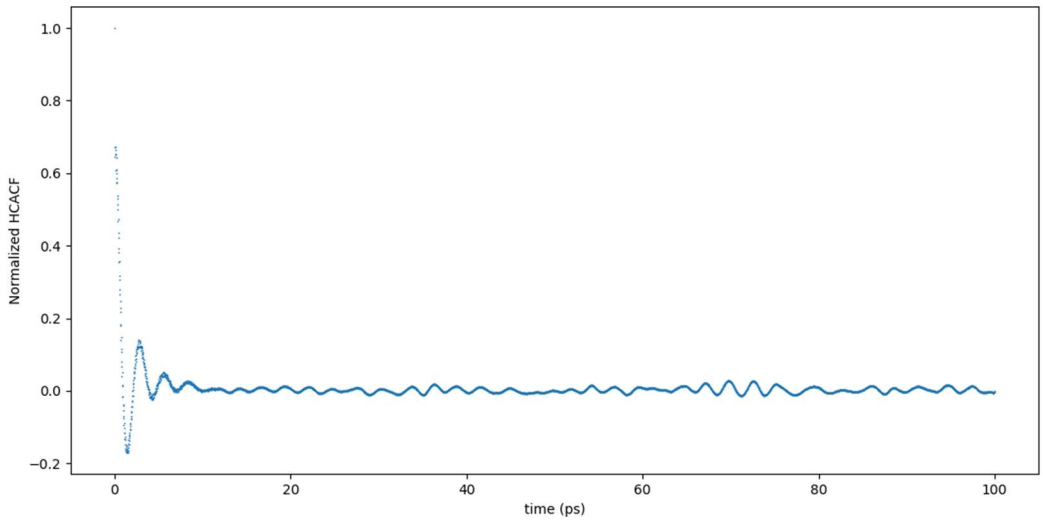

Fig. 3.5(b)

Figure 3.5: Smoothing the raw HCACF data by taking average of heat current autocorrelation functions starting at different t_0 with the same correlation length. (a). Averaged HCACF data for 50 different time periods. (b). Averaged HCACF data for 200 different time periods.

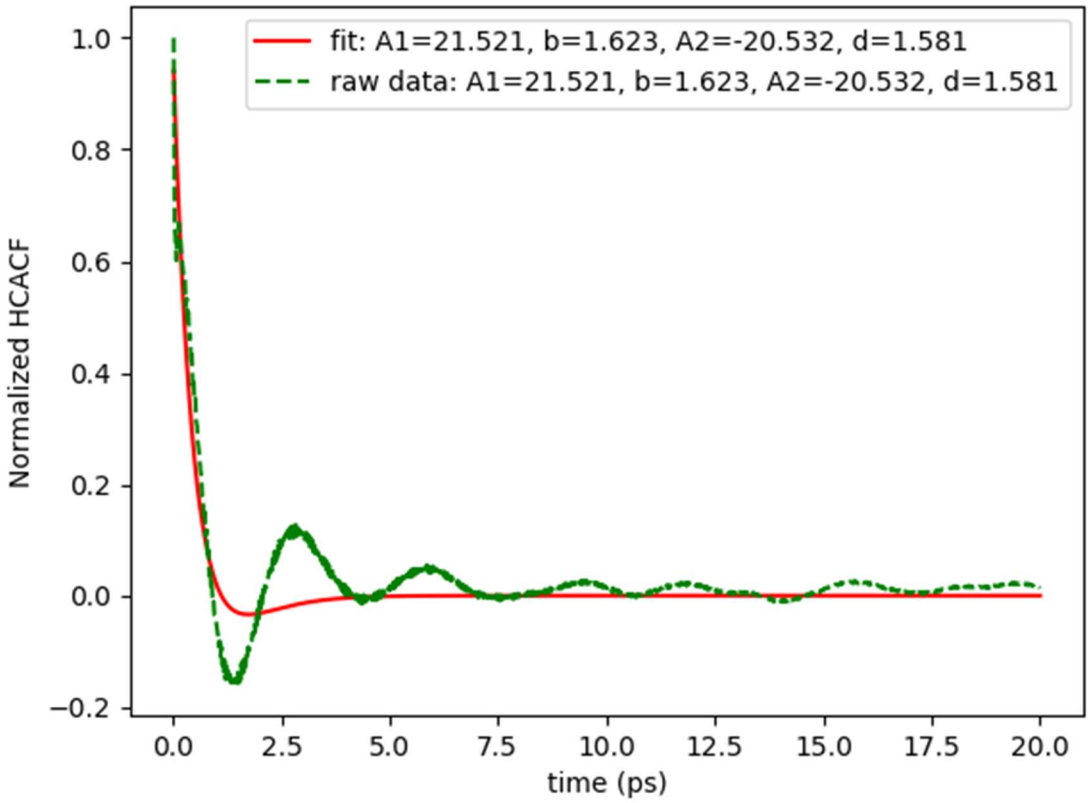

Figure 3.6: Double exponential fitting of normalized HCACF <J(t)J(0)>/<J(0)J(0)> after smoothing.

To obtain the relaxation time of different vibration modes, we fitted the normalized data of HCACF to a double exponential form, as proposed in [28]:

$$C_j^c(t) = \sum_i A_i \exp\left(-\frac{t}{\tau_i}\right) \tag{3.2}$$

where different τ_i denotes different relaxation time of lattice vibration modes. For thermal conductivity calculation, low frequency acoustic lattice vibration modes are known to play a more important part. It is worth noticing that three-dimensional h-BN lattice has six vibration modes, among them three number of acoustic branches could be predicted, including one longitudinal in which the atoms vibrate in one direction of the chain and two transverse ones, in which the atoms

vibrate perpendicularly to the direction of the propagation of the wave, named longitudinal acoustic (LA) and transverse acoustic (TA) branches, respectively. Therefore, there will be one longitudinal acoustic branch and two transverse branches. However, in highly symmetric directions the two transverse modes could probably be degenerated. In this situation, we fit the HCACF to a double exponential form, namely

$$C_j^c(t) = A_1 \exp\left(-\frac{t}{\tau_1}\right) + A_2 \exp\left(-\frac{t}{\tau_2}\right) \tag{3.3}$$

The subscripts 1 and 2 denote longitudinal acoustic modes and transverse acoustic modes. Through the integration of HCACF, we could obtain the value of thermal conductivity by

$$\kappa = \frac{1}{Vk_BT^2}(A_1\tau_1 + A_2\tau_2) \tag{3.4}$$

The parameters A_1 , τ_1 , A_2 , and τ_2 are derived from the first 20 ps using nonlinear least-squares methods, as shown in Fig. 3.6. According to our fitting, $\tau_{1x} = \frac{1}{b} = 0.616\, ps$, $\tau_{2x} = \frac{1}{d} = 0.633\, ps$. For normalized HCACF, the scaling parameter $\langle J(0) \cdot J(0) \rangle$ is calculated to be 541600 in unit $eV^2 \cdot \dot{A}^2 \cdot ps^{-2}$. This set of fitting parameters finally gave us $\kappa_{xx} = 217 W/mK$.

Likewise, applying the above-mentioned method to y direction (armchair direction) gave us $\kappa_{yy} = 191 W/mK$, with phonon relaxation time $\tau_{1y} = 0.551\, ps$, $\tau_{2y} = 0.572\, ps$. One can conclude that the difference of thermal conductivity between zigzag and armchair direction is usually less than 20%.

The simulation result in both x and y directions gave us that the relaxation time of double exponential fitting is around 0.5 to 0.6 ps, which is comparable to the energy of LA and TA phonon modes in the phonon dispersion spectra of monolayer pristine h-BN. And these two modes also have been proved to contribute the most to thermal conductivity.

It is also worth noticing that the size effect of MD simulations has also triggered controversy. Comparisons between nanoribbons of different width and length have been made. And the conclusion is clear from equation (1.5) that in general, phonon-boundary scattering effect in 2-D structures such as graphene, h-BN decreases the lifetime of low-frequency phonon modes. As the relaxation time decreases, the phonon mean-free path of the low-frequency phonons decreases, thus the thermal conductivity also decreases.

Instead of repeating calculation on nanoribbon structures of different length and width, we took a rhombic structure with an edge length of 36.9 nm, namely 45000 atoms in total. Simulation timestep is set to be 1fs. The system is first equilibrated in NVT ensemble for 1ns, then thermodynamic data are collected under NVE ensemble for 5ns. Interestingly, this set of HCACF data showed similar oscillation as that of bulk h-BN structure, as shown in Fig. 3.7. This kind of oscillation could attribute to the lattice structure.

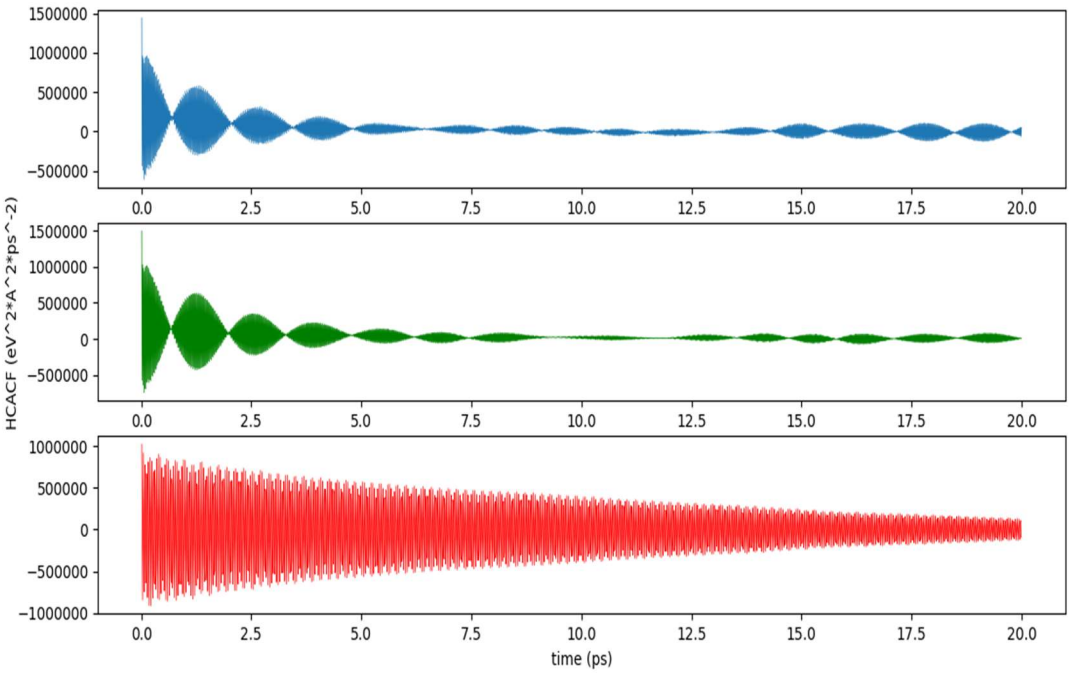

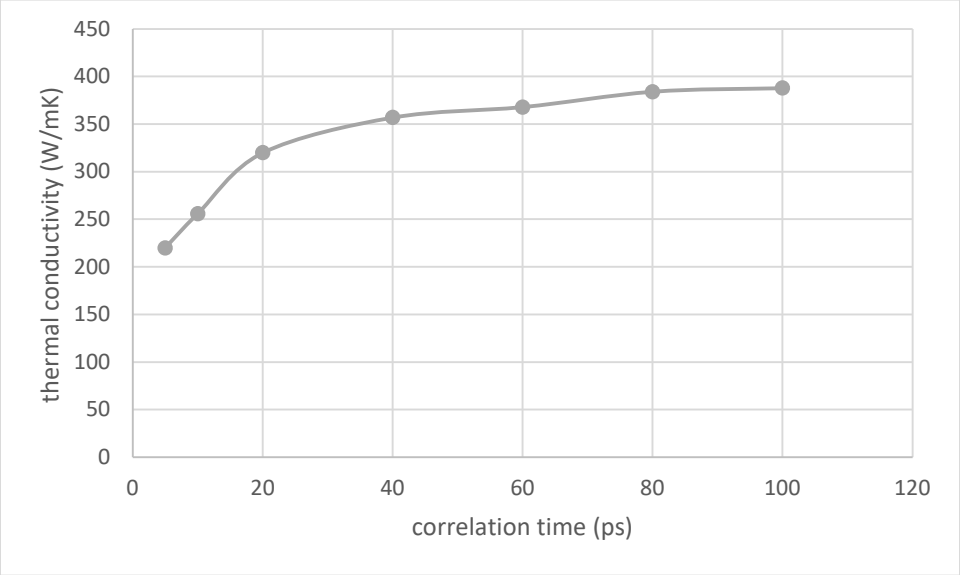

Figure 3.7: The HCACF data along x, y, z direction, denoted in blue, green and red respectively, as well as the thermal conductivity value calculated with different correlation time ranging from to 5 to 100 ps.

As it is shown in the HCACF plot, the oscillation of HCACF in x-y direction is somehow relevant to their relaxation time of different vibration modes. McGaughey et al [33] proposed a method to determine the existence of distinctive vibration modes and their impact on thermal transport based on simulations of different silicon systems. In this case, the HCACF is fitted into the addition of a double exponential part and a set of cosine-related functions to simulate the optical branch of phonons due to multi-atomic unit cells:

$$HCACF = A_{ac,s}\exp\left(-\frac{t}{\tau_{ac,s}}\right) + A_{ac.l}\exp\left(-\frac{t}{\tau_{ac,l}}\right) + \sum_i B_{op,i}\exp\left(-\frac{t}{\tau_{op,i}}\right)\cos\left(\omega_{op,i}t\right) \quad (3.5)$$

Correspondingly, the contribution of all modes to total thermal conductivity would become:

$$\kappa = \frac{1}{Vk_BT^2}\left(A_{ac,s}\tau_{ac,s} + A_{ac,l}\tau_{ac,l} + \sum_i \frac{B_{op,i}\tau_{op,i}}{1+{\tau_{op,i}}^2{\omega_{op,i}}^2}\right) \quad (3.6)$$

where the subscripts s, l is abbreviation of “short range” and “long range”. By this formula, the sinusoidal vibration could be represented, and thus it turns out to be possible to examine the

contribution of all kinds of possible phonon vibration modes together. And if we define the conception of "cage" by the time difference between neighboring "wave packets", then the "distance" between two adjacent peaks that are in the same cage should be relevant to two times of $\tau_{ac,sh}$, possibly meaning the time that energy need to pass through B-N-B pairs. It is worth noticing that the thermal conductivity calculated with this system had larger value of thermal conductivity compared with that computed from the former model. This may indicate that the contribution of optical phonon modes in h-BN to its thermal conductivity is not negligible. Although the reason why different shape of HCACF could appear with different shape of unit cell and different structure of simulation systems is still not clear, more detailed study is required to illustrate this problem.

3.2.2 Applying NEMD methods

Compared with EMD method that applied Green-Kubo formula and linear response theory, NEMD method is known for its simplicity. In this section, we simulated a h-BN nano-stripe with 196.8 nm in length (x direction) and 12.8 nm in width. The stripe is divided into 20 regions along x direction. Hot bath is set in the central part of this stripe, while cold bath is set in the ending part of this stripe. The temperature of each region is measured, with its location denoted as the coordinate of the central point of this district. Simulation timestep is set to be 1 fs. The system is first heat balanced under NVT ensemble for 1ns, then the middle regions between hot and cold bath region are set under NVE ensemble to guarantee that energy flows to both sides do not dissipate due to heat exchange with the simulation "environment". Heat flux data are automatically collected every 10 timesteps, and after taking the average of 10000 heat flux data, the mean value

is treated as the heat flux at t = 0.1 ns. Since the data collection time is 1 ns, ten values are recorded in total. The temperature data is calculated in the same method.

Fig. 3.8. showed the relation between temperature of each region and its corresponding location, given heat bath T_h = 325K and cold bath T_c = 275K. Since the heat flow is split into two opposite directions due to the periodic boundary condition, only one set of regions between hot bath and cold bath are taken into consideration.

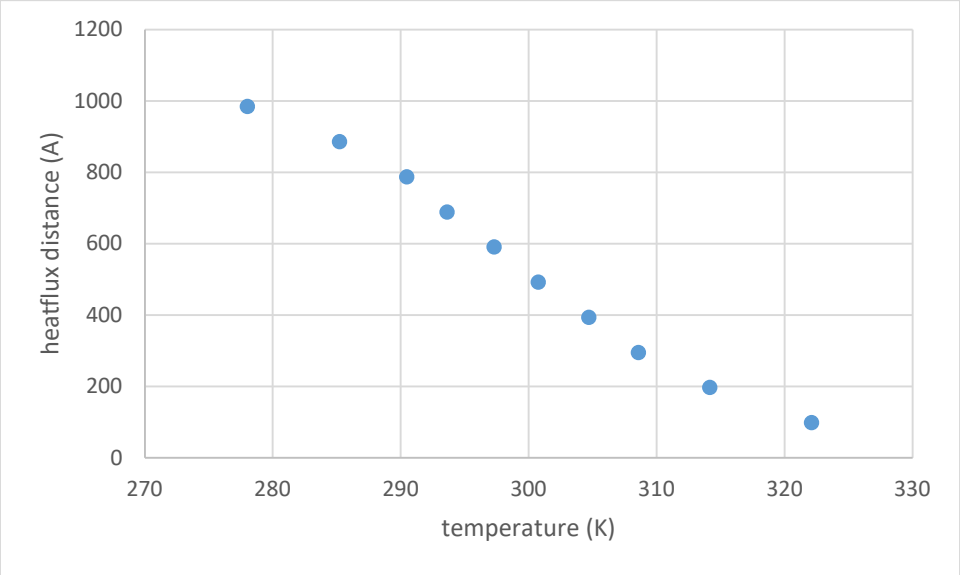

Figure 3.8: Temperature – coordinate relation given by direct NEMD method.

Applying Fourier's law immediately gave us: $\kappa = -J \cdot (\frac{\Delta x}{\Delta T})$. The inverse temperature gradient is fitted with the data in the middle part of this plot. The calculated thermal conductivity along x direction equals 286 W/mK.

This NEMD run is then repeated several times with different temperature gradient (initial temperature of T_c and T_h) to make sure that the calculated value of thermal conductivity is not impacted by temperature gradient. The raw data of heat flux J is listed in the Tab. 3.1.

T/K (range)	[290,310]	[280,320]	[275,325]	[295,315]	[270,330]	Region center
Sample	1	2	3	4	5	Coordinate in x direction
averaged_Jx	0.00261	0.00532	0.00657	0.00285	0.00741	
C1 (temp)	309.621	318.09	322.11	314.36	326.41	98.4
C2	305.95	311.51	314.17	311	317.37	196.8
C3	303.5	307.42	308.58	309.1	311.21	295.2
C4	301.95	303.83	304.7	307.28	306.24	393.6
C5	300.62	300.75	300.75	305.19	301.34	492
C6	299.22	298.07	297.3	303.57	296.92	590.4
C7	297.76	294.99	293.63	302.3	292.97	688.8
C8	296.23	291.9	290.48	300.75	288.46	787.2
C9	294.26	287.72	285.21	298.84	282.62	885.6
C10	290.67	282.1	278.02	295.48	273.63	984

Table 3.1: Data of direct NEMD simulation with different initial temperature gradients. Temperature gradient is calculated with data in the middle part ranging from C3 to C8.

It is worth noticing though, one major concern about NEMD method appeared to be the large systematic error in the measurement of direct heat flux J. The value of J measured by this method could vary drastically due to the instability of local structure.

Timestep	Sample 1	Sample 2	Sample 3	Sample 4	Sample 5
100000	0.003714	0.005991	0.007681	0.004132	0.008772
200000	0.000965	0.001603	0.006397	0.001344	0.007307
300000	0.005783	0.007317	0.006497	0.004471	0.007282
400000	-0.0005	0.003726	0.004976	0.002808	0.008592
500000	0.001574	0.005859	0.004508	-0.00013	0.004975
600000	0.003632	0.004493	0.007769	0.003345	0.006447
700000	0.002545	0.00742	0.006027	0.003273	0.009486
800000	0.004272	0.006304	0.008135	0.004007	0.010185

Table 3.2: The standard deviation of LAMMPS calculated value of heat flux along x direction.

900000	0.002356	0.004971	0.008835	0.002134	0.005919
1000000	0.001748	0.005489	0.004907	0.003097	0.005117
mean value of J_x	0.00261	0.00532	0.00657	0.00285	0.00741
standard deviation	0.001713	0.001652	0.001419	0.001333	0.001721

Table 3.2 Continued: The standard deviation of LAMMPS calculated value of heat flux along x direction.

As it is shown in Tab. 3.2, the maximum percentage of standard deviation of heat flux could reach to 65% in sample 1, the minimum percentage found in sample 3 also exceeds 20%. For both sample with $\Delta T = 20K$ (sample 1 and sample 4), local heat flux sometimes even turned out to be negative! It is impossible that heat could flow back from low temperature region to high temperature region! In converse, the local heat flux data of samples with initial $\Delta T > 50K$ (sample 3 and sample 5) showed more stability, indicating that the heat flux data of samples with larger initial temperature gradient are more likely to render reliable results. But even if ΔT in this simulation is only 20K, the temperature gradient would exceed 10^8 K/m, which is impossible in reality, since the system would collapse before heat could transfer inside it (too much atomic kinetic energy)! Therefore, although the result of thermal conductivity seems plausible, it is still very dangerous to apply direct NEMD method in nanoscale. Generally speaking, NEMD method that applies Fourier's law directly serve as a better fit for larger-scaled, probably continuum materials simulations.

Although there exist flaws of direct method that makes it unsuitable for nanoscale modeling, Fourier's Law still plays an important part in heat transport mechanism. In recent years amendments of direct methods proposed, among which the reversible non-equilibrium molecular dynamics (R-NEMD) method drew much attention. This kind of NEMD has the prerequisite of (kinetic) energy swap between two regions to create and record corresponding heat flux, before

Fourier's Law is applied to get the exact value of thermal conductivity. The mechanism of this method is introduced in Chapter 2, section 2.3.2. The size of h-BN nano stripe system that we applied in this simulation is the same as the above-mentioned one. Timestep is set as 1 fs, and the system is first thermal equilibrated in NVT ensemble for 1 ns, with T=300K. Then it is equilibrated in NVE ensemble for 1 ns before temperature gradient is exerted to this system by swapping of atomic velocities along thermal transport direction. The data is collected every 10 timesteps, and are then averaged every 100 ps. Data collection process lasted for 2 ns. We could get the raw data describing how velocity exchange between the cold bath and the hot bath intrigued the appearance of heat flux:

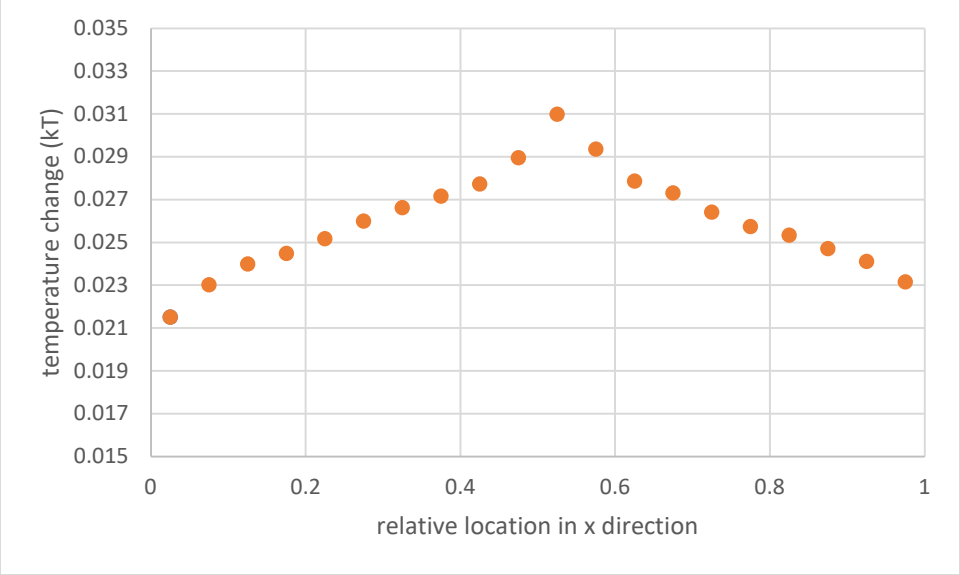

Figure 3.9: The raw data of R-NEMD method proposed by Muller Plathe under room temperature. Temperature change versus the relative location in heat flowing direction (x direction). Bin size is set to be 20, and the hot/cold bath is located in the middle (bin = 11) and the side (bin = 1).

Applying Fourier's Law gave us the thermal conductivity calculated by R-NEMD methods, we have a thermal conductivity value of for such a system about 264W/mK. But it is worth noticing that the calculation of temperature gradient should be linear fitted with the whole set of data instead

of only selecting the more linear looking part in the middle of our simulation system. This is because the heat flow is given directly by the velocity exchange between cold and hot baths. Despite the similarity in thermal conductivity value given by direct NEMD method and R-NEMD methods, R-NEMD methods obviously has more advantage in terms of simulation in nanoscale. By applying R-NEMD method, the local stability is somehow guaranteed, since energy exchange only happened directly between the hot bath and the cold bath. The total energy could also be better conserved. In this way, the temperature gradient could still reach to 10^8 K/m to 10^9 K/m, a "moderate" temperature gradient suitable for MD calculations. And the concept of "reversible" somehow indicates that the energy swapping could be done in both way (either making the cold bath colder or hotter).

4. CONCLUSION

In this study, we tried to provide a thorough understanding of how different molecular dynamic simulation methods functioned, by giving an example of its application in multiple hexagonal boron nitride systems. Firstly, we simulated bulk h-BN systems with LJ potential as the interlayer force field, and Tersoff potential as the in-plane force field applying EMD method. Simulation result showed that thermal equilibrated bulk h-BN systems tend to pack in A-B stacking. The bulk thermal conductivity under room temperature is calculated to be 173.9W/mK and 180.0W/mK in x and y direction, and 5.3W/mK in perpendicular direction. This result showed consistence with former experiments, leading to the conclusion that a combination of Tersoff potential and LJ potential remains the most efficient way to describe bulk crystalline honeycomb structures. However, the weight of Coulombic interaction part in interlayer atomic interactions and its contribution to both steady-state lattice structure and thermal conductivity still remain unveiled.

We also simulated monolayer pristine h-BN systems with both rectangular shape and rhombic shape, leading to different unit cells, consequently. We also fitted the corresponding HCACF to double exponential form. The thermal conductivity value is calculated by integrating the fitting curve of HCACF. At temperature T=300K, the thermal conductivity of a rectangular shaped h-BN nanosheet is around 200W/mK in x-y plane, slightly larger than that of bulk structure. This is reasonable since the presence of LJ potential help localized the atom, restricting the phonon vibration thus limiting the thermal conductivity. However, it is worth noticing that the shape of the simulation system may have an impact on the final result, since the thermal conductivity calculated by LAMMPS for rhombic h-BN system at room temperature surprisingly gave a larger kappa (over 300W/mK). It may be possible to let the random convergence of LAMMPS automatically reported result to take the blame. On the other hand, however, the difference in

oscillation modes of heat current auto-correlation functions is also noticed. This difference may due to the triangular unit cell in rhombic simulation systems. Detailed information of distinctive phonon vibration modes could possibly be inferred from oscillation of HCACF. The relaxation time of phonon modes given by double exponential fitting is around 0.55 to 0.65 ps, which showed vibration process energetically analogous to the LA and TA phonon dispersion relation spectra curve reported by former research. And it is clear that low frequency phonon vibration modes played the most important part in heat transport.

We also applied NEMD methods to pristine h-BN nano stripe system at T = 300K. It showed about 20% to 30% percent larger value of thermal conductivity in terms of result. These methods are known for its convenience in data post processing and efficiency. And although the result showed no obvious difference, R-NEMD methods seems to be more convincing since it better stabilizes the simulation system, which is very helpful in maintaining energy conservation of certain simulation system.

In short, we provided another perspective for the application of different molecular dynamics methods in pristine h-BN structures. Clearly, more theoretical research pertaining to h-BN are necessary since there exists much more kinds of h-BN systems, including defective and polycrystalline systems. Besides, the implementation of different molecular dynamics methods and the physics beneath the output is essential, especially for EMD simulation, for it is known to be widely applicable to many atomic systems. Moreover, comparison between calculations based on DFT theory, ab initio molecular dynamic methods and classical molecular dynamic methods may also give some meaningful results.

REFERENCES

[1]. L. Duclaux et al. “Structure and low-temperature thermal conductivity of pyrolytic boron nitride,” *Phys Rev B* **46**, 3362 (1992).

[2]. Insun Jo et al. “Thermal Conductivity and Phonon Transport in Suspended Few-Layer Hexagonal Boron Nitride,” *Nano Lett* **13**, 550-554 (2013).

[3]. E. K. Sichel et al. “Heat capacity and thermal conductivity of hexagonal pyrolytic boron nitride,” *Phys Rev B* **13**, 4607 (1976).

[4]. Haiqing Zhou et al. “High thermal conductivity of suspended few-layer hexagonal boron nitride sheets,” *Nano Research* 2014, 7(8): 1232–1240.

[5]. Qiran Cai et al. “High thermal conductivity of high-quality monolayer boron nitride and its thermal expansion,” *Sci. Adv.* **5**: 0129 (2019).

[6]. L. Lindsay, D. A. Broido. “Enhanced thermal conductivity and isotope effect in single-layer hexagonal boron nitride,” *Phys Rev B*. **84**, 155421 (2011).

[7]. D. L. Nika et al. “Phonon thermal conduction in graphene: Role of Umklapp and edge roughness scattering,” *Phys Rev* B **79**, 155413 (2009).

[8]. Steve K. Jacimovski et al. “Phonon thermal conductivity of graphene,” *Superlattices and Microstructures* **88**, 330-337 (2015).

[9]. J. M. Dickey et al. “Computer Simulation of the Lattice Dynamics of Solids,” *Phys Rev.* **188**, 1407-1418 (1969).

[10]. Alper Kınacı et al. “Thermal conductivity of BN-C nanostructures,” *Phys Rev* B **86**, 115410 (2012).

[11]. C. Sevik, A. Kinaci, J. B. Haskins, and T. Çağın, “Characterization of thermal transport in low-dimensional boron nitride nanostructures,” *Phys Rev* B **84**, 085409 (2011).

[12]. J. H. Los et al. “Extended Tersoff potential for boron nitride: Energetics and elastic properties of pristine and defective h-BN,” *Phys Rev B* **96**, 184108 (2017).

[13]. Tal Maaravi et al. “Interlayer Potential for Homogeneous Graphene and Hexagonal Boron Nitride Systems: Reparametrization for Many-Body Dispersion Effects,” *J. Phys. Chem. C* 121, 22826-22835 (2017).

[14]. Yuanyue Liu et al. “Dislocations and Grain Boundaries in Two-Dimensional Boron Nitride,” *ACS Nano* **6**(8): 7053-7058 (2012).

[15]. Timon Rabczuk et al. “Thermal Conductance along Hexagonal Boron Nitride and Graphene Grain Boundaries,” *Energies*. **11**, 1553 (2018).

[16]. Alireza Tabarraei. “Thermal conductivity of monolayer hexagonal boron nitride nanoribbons,” *Comp. Mat. Sci.* **108** 66-71 (2015).

[17]. Bohayra Mortazavi et al. “Modelling heat conduction in polycrystalline hexagonal boron-nitride films,” *Scientific Reports*. **5,** 13228 (2015).

[18]. L. Verlet. “Computer experiments on classical fluids. I. thermodynamical properties of Lennard-Jones molecules,” *Phys. Rev*. **159**: 98-103 (1967).

[19]. Michael P. Allen, “*Introduction to Molecular Dynamics Simulation*,” Computational Soft Matter: From Synthetic Polymers to Proteins, Lecture Notes, NIC Series, **23**: 1-28 (2004).

[20]. R. Kubo. “The fluctuation-dissipation theorem,” *Rep. Prog. Phys.* **29,** 255 (1966).

[21]. Denis J. Evans & Gary P. Morriss, “*Statistical Mechanics of Nonequilibrium Liquids*. *Chapter 4: The Green Kubo Relations*,” ANU Press. (2007).

[22]. Jianwei Che et al. “Thermal conductivity of diamond and related materials from molecular dynamics simulations,” *J. Chem. Phys.* **113**, 6888 (2000).

[23]. Florian Muller Plathe. “A simple nonequilibrium molecular dynamics method for calculating the thermal conductivity,” J. Chem. Phys. **106**, 6082 (1997).

[24]. A. K. Rappe et al. “UFF, a Full Periodic Table Force Field for Molecular Mechanics and Molecular Dynamics Simulations,” *J. Am. Chem. SOC.* **114**, 10024-10039 (1992).

[25]. J. Tersoff. “New empirical approach for the structure and energy of covalent systems,” *Phys. Rev. B*. **37**, 6991-7000 (1988).

[26]. Jinlong He et al. “Thermal transport in monocrystalline and polycrystalline lithium cobalt oxide,” *Phys. Chem. Chem. Phys*. **21**, 12192 (2019).

[27]. A. J. H. McGaughey et al. “Thermal conductivity decomposition and analysis using molecular dynamics simulations: Part II. Complex silica structures,” *Int. J. Heat Mass Transfer.* **47**, 1799–1816 (2004).

[28]. Justin Haskins et al. “Equilibrium limit of thermal conduction and boundary scattering in nanostructures,” *J. Chem. Phys.* **140**, 244112 (2014).

APPENDIX

In this study, all the data collection is based on LAMMPS software. The code for Green-Kubo method that we applied for bulk h-BN system in this work is posted below:

```
variable x equal 10
variable y equal 10
variable z equal 2
variable t equal 300.0         # temperature
variable p equal 2000          # correlation length
variable s equal 10            # sample interval
variable d equal 20000         # dump interval
variable a equal 1.44          # lattice setting
variable b equal $a*3
variable c equal $a*sqrt(3)
variable e equal 3.35*2
variable f equal 1.0/6.0
variable g equal 2.0/3.0

units          metal
timestep       0.0005          # dt = 0.5fs
atom_style     atomic

lattice custom 1.0  a1 $b 0 0  a2 0 $c 0  a3 0 0 $e   &
                    basis 0  0   0   basis 0.5 0.5 0   &
                    basis $f 0.5 0   basis $g  0   0   &
                    basis 0  0  0.5  basis 0.5 0.5 0.5 &
                    basis $f 0.5 0.5 basis $g  0  0.5

region myreg block 0 $x 0 $y 0 $z
create_box    4 myreg
create_atoms  4 region myreg basis 1 1 basis 2 1 &
                             basis 3 2 basis 4 2 &
                             basis 5 3 basis 6 3 &
                             basis 7 4 basis 8 4

mass 1 10.81
mass 2 14.007
mass 3 14.007
mass 4 10.81

velocity all create $t 187265 dist gaussian rot yes mom yes

pair_style hybrid/overlay tersoff lj/cut 16.0       # LJ global cutoff
pair_coeff * * tersoff BN.tersoff B N B N
pair_coeff 1 3 lj/cut 0.00484 3.449        # set the epsilon and sigma
pair_coeff 2 4 lj/cut 0.00484 3.449
pair_coeff 1 4 lj/cut 0.00781 3.638
pair_coeff 2 3 lj/cut 0.003   3.261
```

```
neighbor          2.0 bin
neigh_modify      delay 0 every 1

# first equilibrium run
fix       1 all nvt temp 300.0 300.0 1.0
thermo    $d
run       1000000
unfix     1

# thermal conductivity calculation
reset_timestep 0

compute    myKE   all   ke/atom
compute    myPE   all   pe/atom
compute  myStress all stress/atom NULL virial
compute    flux   all  heat/flux  myKE myPE myStress

variable f1 equal c_flux[1]
variable f2 equal c_flux[2]
variable f3 equal c_flux[3]
variable time equal step*dt

fix heatcurrent all print 1 "${time} ${f1} ${f2} ${f3}" file &
HC_thermoInfo.txt screen no                    # record heat flux data

fix JJ all ave/correlate $s $p $d c_flux[1] c_flux[2] c_flux[3] &
       type auto file profile.heatflux ave running

variable scale equal $s*dt/$t/$t/vol
variable kb equal 8.6172e-5         # Boltzmann constant in unit metal
variable k11 equal trap(f_JJ[3])*${scale}/${kb}
variable k22 equal trap(f_JJ[4])*${scale}/${kb}
variable k33 equal trap(f_JJ[5])*${scale}/${kb}

thermo  $d
thermo_style custom step temp v_k11 v_k22 v_k33

# dump to Ovito
dump 3 all custom $d dump.kappa.* type xs ys zs vx vy vz fx fy fz

run   4000000
print "result of x y z conductivity: ${k11} ${k22} ${k33}"
print "units of kappa: eV/(A*ps*K) "
undump 3
unfix  JJ
unfix  1
print "All done!"
```